 CMES, vol.107, no.2, pp.81-101, 2015

A Micromechanical Model for Estimating the Effective Stiffness of a Pair of Micro-cracked Interfaces in an Orthotropic Trimaterial under Inplane Deformations

X. Wang[1], W.T. Ang[1,2], H. Fan[1]

Abstract: A micromechanical model is proposed here for estimating the effective stiffness of a pair of parallel microscopically damaged interfaces in a trimaterial under inplane elastostatic deformations. The trimaterial is made of an orthotropic thin layer sandwiched between two orthotropic half-spaces. The microscopically damaged interfaces are modeled using periodically distributed interfacial micro-cracks. The micromechanical model is formulated and numerically solved in terms of hypersingular boundary integro-differential equations. The effects of the width of the thin layer, the micro-crack densities of the two interfaces and the material constants of the thin layer and the two half-spaces on the effective stiffness coefficients are investigated.

Keywords: Micromechanics; Microscopically damaged interface; Effective stiffness coefficients; Trimaterial; Thin film; Hypersingular integral and integro-differential equations.

1 Introduction

Multilayered structures are widely used in microelectromechanical devices such as micro-sensors and actuators (Muralt (2000)). During the fabrication of such structures, micro-cracks may be formed on the interface between two dissimilar layers due to mismatch in the thermal and mechanical properties of the layers or micro-roughness of surfaces.

For a simplified analysis of multilayered materials, a micro-cracked interface may be modeled as a continuous distribution of springs characterized by a set of stiffness coefficients. As in Benveniste and Miloh (2001), the tractions on the spring-like interface are linearly related to the jump in the displacements across opposite sides

[1] School of Mechanical and Aerospace Engineering, Nanyang Technological University, Singapore
[2] Author for correspondence, http://www.ntu.edu.sg/home/mwtang/, Email: mwtang@ntu.edu.sg

of the interface, that is, if the spring-like interface between two dissimilar materials referred to as 1 and 2 is denoted by Γ then the interfacial conditions are given by

$$\underline{\underline{\boldsymbol{\sigma}}}^{(1)} \cdot \underline{\mathbf{n}} = \underline{\underline{\boldsymbol{\sigma}}}^{(2)} \cdot \underline{\mathbf{n}} = \underline{\underline{\mathbf{k}}} \cdot (\underline{\mathbf{u}}^{(1)} - \underline{\mathbf{u}}^{(2)}) \text{ on } \Gamma, \tag{1}$$

where $\underline{\mathbf{n}}$ is the unit normal vector to Γ pointing into material 1, $\underline{\mathbf{u}}^{(i)}$ and $\underline{\underline{\boldsymbol{\sigma}}}^{(i)}$ are respectively the displacement (first order tensor) and the stress (second order tensor) in material i and $\underline{\underline{\mathbf{k}}}$ is the stiffness (second order tensor) of Γ.

The spring-like interface defined by (1) was used by many researchers for analyzing multilayered materials with imperfect weak interfaces (see, for example, Ang (2007), Fan and Wang (2003), Jones and Whittier (1967), Margetan, Thompson and Gray (1988) and Sudak and Wang (2006)). There are, however, very few papers that estimate the stiffness $\underline{\underline{\mathbf{k}}}$ by considering the micro details of the interface.

To estimate the effective stiffness of a micro-cracked interface between two half-spaces, Fan and Sze (2001) proposed a finite element based three-phase model in which the interface was modeled by a representative micro-crack interacting with spring-like effective regions with an unknown stiffness. The micro-crack details captured in the highly simplified three phase model were the average micro-crack length and the micro-crack density. More recently, Wang, Ang and Fan (2012) and Wang, Fan and Ang (2014) estimated the effective stiffness by simulating statistically the interfacial micro-cracks between two anisotropic elastic half-spaces under antiplane deformations. The positions and the lengths of the micro-cracks were randomly chosen. The micromechanical-statistical approach in Wang, Ang and Fan (2012) and Wang, Fan and Ang (2014) was also used in Wang, Ang and Fan (2015) to compute the effective stiffness of a micro-cracked interface between an orthotropic thin layer and an orthotropic half-space under inplane deformations.

The current paper proposes a micromechanical model for the estimation of the effective stiffness of a pair of parallel micro-cracked interfaces in a trimaterial under inplane elastostatic deformations. The trimaterial is made of an orthotropic thin layer sandwiched between two orthotropic half-spaces. The micro-cracks on the parallel plane interfaces are periodically distributed. The micro-crack density of one of the interfaces may be different from that of the other interface. The task of calculating the effective stiffness of the micro-cracked interfaces is eventually reduced to solving numerically a system of hypersingular boundary integro-differential equations. The effects of the width of the thin layer, the micro-crack densities of the two interfaces and the material constants of the thin layer and the two half-spaces on the effective stiffness coefficients are investigated in some details.

The hypersingular integral approach is widely used for solving elastic crack problems (see Ang (2013), Purbolaksono and Aliabadi (2005), Sanz, Solis and Dominguez

(2007) and other references therein). It is advantageous for use here as the crack-opening displacements which are required in computing the effective stiffness of the micro-cracked interfaces appear directly in the hypersingular integro-differential equations for the conditions on the micro-cracks.

2 Statement of the micromechanical problem

With reference to a Cartesian coordinate system $Ox_1x_2x_3$, consider a thin elastic layer in the region $0 < x_2 < h$ sandwiched between two elastic half-spaces which occupy the regions $x_2 < 0$ and $x_2 > h$. The materials in the layer and the two half-spaces are orthotropic, having possibly dissimilar elastic properties. The plane interfaces $x_2 = 0$ and $x_2 = h$ between the layer and the half-spaces are denoted by I and II respectively.

Each of the interfaces contains a periodic distribution of micro-cracks which have the geometries independent of the x_3 coordinate. More specifically, the micro-cracks on interface I lie in the regions

$$a_{\mathrm{I}}^* + nL < x_1 < b_{\mathrm{I}}^* + nL,\ x_2 = 0\ (n = 0, \pm 1, \pm 2, \ldots),$$

and those on interface II lie in

$$a_{\mathrm{II}}^* + nL < x_1 < b_{\mathrm{II}}^* + nL,\ x_2 = h\ (n = 0, \pm 1, \pm 2, \ldots),$$

where L is the length of a period interval of the micro-cracked interface, a_{I}^*, b_{I}^*, a_{II}^* and b_{II}^* are real numbers such that $0 < a_{\mathrm{I}}^* < b_{\mathrm{I}}^* < L$, $0 < a_{\mathrm{II}}^* < b_{\mathrm{II}}^* < L$ and $a_{\mathrm{I}}^* + b_{\mathrm{I}}^* = a_{\mathrm{II}}^* + b_{\mathrm{II}}^* = L$. Thus, interfaces I and II contain periodic arrays of evenly distributed micro-cracks of length $2a_{\mathrm{I}}$ and $2a_{\mathrm{II}}$ respectively, where $a_{\mathrm{I}} = (b_{\mathrm{I}}^* - a_{\mathrm{I}}^*)/2$ and $a_{\mathrm{II}} = (b_{\mathrm{II}}^* - a_{\mathrm{II}}^*)/2$. The materials in the layer and the half-spaces are assumed to be perfectly bonded on the uncracked parts of the interfaces. Refer to Fig. 1 for a geometrical sketch of the trimaterial.

The damage ratios ρ_{I} and ρ_{II} which give the micro-crack densities of interfaces I and II are defined as follows:

$$\rho_{\mathrm{I}} = \frac{2a_{\mathrm{I}}}{L} \text{ and } \rho_{\mathrm{II}} = \frac{2a_{\mathrm{II}}}{L}. \tag{2}$$

The trimaterial undergoes an inplane elastostatic deformation governed by the partial differential equations

$$\begin{aligned} C_{11}(x_2)\frac{\partial^2 u_1}{\partial x_1^2} + [C_{12}(x_2) + C_{66}(x_2)]\frac{\partial^2 u_2}{\partial x_1 \partial x_2} + C_{66}(x_2)\frac{\partial^2 u_1}{\partial x_2^2} = 0, \\ C_{66}(x_2)\frac{\partial^2 u_2}{\partial x_1^2} + [C_{12}(x_2) + C_{66}(x_2)]\frac{\partial^2 u_1}{\partial x_1 \partial x_2} + C_{22}(x_2)\frac{\partial^2 u_2}{\partial x_2^2} = 0, \end{aligned} \tag{3}$$

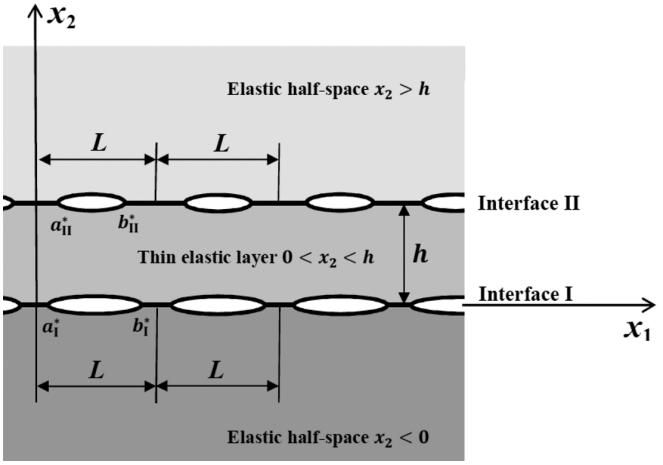

Figure 1: A geometrical sketch of the trimaterial and the micro-cracked interfaces

where $u_1(x_1,x_2)$ and $u_2(x_1,x_2)$ are the x_1 and x_2 Cartesian components of the displacement and $C_{11}(x_2),C_{12}(x_2),C_{22}(x_2)$ and $C_{66}(x_2)$ are elastic moduli defined by

$$(C_{11}(x_2),C_{22}(x_2),C_{12}(x_2),C_{66}(x_2)) = \begin{cases} \left(C_{11}^{(1)},C_{22}^{(1)},C_{12}^{(1)},C_{66}^{(1)}\right) & \text{for } x_2 > h, \\ \left(C_{11}^{(2)},C_{22}^{(2)},C_{12}^{(2)},C_{66}^{(2)}\right) & \text{for } 0 < x_2 < h, \\ \left(C_{11}^{(3)},C_{22}^{(3)},C_{12}^{(3)},C_{66}^{(3)}\right) & \text{for } x_2 < 0, \end{cases} \tag{4}$$

with $C_{11}^{(p)},C_{22}^{(p)},C_{12}^{(p)}$ and $C_{66}^{(p)}$ $(p=1,2,3)$ being positive constants such that

$$C_{11}^{(p)}\xi_1^2 + C_{22}^{(p)}\xi_2^2 + 2C_{12}^{(p)}\xi_1\xi_2 + C_{66}^{(p)}\xi_3^2 > 0 \tag{5}$$

for all real numbers ξ_1,ξ_2 and ξ_3 such that $\xi_1^2+\xi_2^2+\xi_3^2 \neq 0$.

For the orthotropic trimaterial, if the micro-cracked interfaces I and II are simplified as spring-like interfaces then the interfacial conditions on $x_2 = 0$ and $x_2 = h$ are respectively given by

$$\begin{aligned} k_{1I}[u_1(x_1,0^+) - u_1(x_1,0^-)] &= \sigma_{12}(x_1,0^+) = \sigma_{12}(x_1,0^-), \\ k_{2I}[u_2(x_1,0^+) - u_2(x_1,0^-)] &= \sigma_{22}(x_1,0^+) = \sigma_{22}(x_1,0^-), \end{aligned} \tag{6}$$

and

$$\begin{aligned} k_{1II}[u_1(x_1,h^+) - u_1(x_1,h^-)] &= \sigma_{12}(x_1,h^+) = \sigma_{12}(x_1,h^-), \\ k_{2II}[u_2(x_1,h^+) - u_2(x_1,h^-)] &= \sigma_{22}(x_1,h^+) = \sigma_{22}(x_1,h^-), \end{aligned} \tag{7}$$

where $k_{r\mathrm{I}}$ and $k_{r\mathrm{II}}$ $(r = 1, 2)$ are the effective stiffness coefficients of interfaces I and II respectively and σ_{kj} are the Cartesian components of the stress. For the spring-like interfaces given by (6) and (7) to be valid, the remote external tensile load acting on the trimaterial along the x_2 direction is assumed to be sufficiently large (dominant). The micro-cracks are assumed to be traction free under the remote external load.

The problem is to estimate the effective stiffness coefficients $k_{r\mathrm{I}}$ and $k_{r\mathrm{II}}$ and to investigate the effects of the width h of the layer, the damage ratios ρ_{I} and ρ_{II} and the elastic moduli $C_{11}^{(p)}$, $C_{22}^{(p)}$, $C_{12}^{(p)}$ and $C_{66}^{(p)}$ on $k_{r\mathrm{I}}$ and $k_{r\mathrm{II}}$.

3 Boundary value problem

The boundary value problem to solve for estimating the effective stiffness coefficients $k_{r\mathrm{I}}$ and $k_{r\mathrm{II}}$ of interfaces I and II is stated below.

The displacement u_k and the stress σ_{kj} in the trimaterial are written as

$$\begin{aligned} u_r &= u_r^{(\mathrm{ext})} + u_r^{(\mathrm{imp})}, \\ \sigma_{rj} &= \sigma_{rj}^{(\mathrm{ext})} + \sigma_{rj}^{(\mathrm{imp})}, \end{aligned} \tag{8}$$

where $u_r^{(\mathrm{ext})}$ and $\sigma_{rj}^{(\mathrm{ext})}$ are respectively the displacement and the stress in the trimaterial for the corresponding case in which the interfaces $x_2 = 0$ and $x_2 = h$ are perfect not having any micro-crack and $u_r^{(\mathrm{imp})}$ and $\sigma_{rj}^{(\mathrm{imp})}$ are elastic fields induced by the micro-cracks to satisfy the traction free conditions on the micro-cracks.

Thus, the conditions on the micro-cracked interfaces I and II are given by

$$\begin{aligned} &\sigma_{r2}^{(\mathrm{imp})}(x_1, 0^{\pm}) = -\sigma_{r2}^{(\mathrm{ext})}(x_1, 0) \text{ for } (x_1, 0) \in C_{\mathrm{I}}, \\ &\sigma_{r2}^{(\mathrm{imp})}(x_1, h^{\pm}) = -\sigma_{r2}^{(\mathrm{ext})}(x_1, h) \text{ for } (x_1, h) \in C_{\mathrm{II}}, \\ &\left.\begin{aligned} \Delta u_{r\mathrm{I}}^{(\mathrm{imp})}(x_1) &= 0 \\ \sigma_{r2}^{(\mathrm{imp})}(x_1, 0^{+}) &= \sigma_{r2}^{(\mathrm{imp})}(x_1, 0^{-}) \end{aligned}\right\} \text{ for } (x_1, 0) \in P_{\mathrm{I}}, \\ &\left.\begin{aligned} \Delta u_{r\mathrm{II}}^{(\mathrm{imp})}(x_1) &= 0 \\ \sigma_{r2}^{(\mathrm{imp})}(x_1, h^{+}) &= \sigma_{r2}^{(\mathrm{imp})}(x_1, h^{-}) \end{aligned}\right\} \text{ for } (x_1, h) \in P_{\mathrm{II}}, \end{aligned} \tag{9}$$

where C_{I} and C_{II} denote the micro-cracked parts of interfaces I and II respectively, P_{I} and P_{II} denote the perfectly bonded parts of interfaces I and II respectively, and $\Delta u_{r\mathrm{I}}^{(\mathrm{imp})}(x_1)$ and $\Delta u_{r\mathrm{II}}^{(\mathrm{imp})}(x_1)$ are respectively the displacement jumps $u_r^{(\mathrm{imp})}(x_1, 0^{+}) - u_r^{(\mathrm{imp})}(x_1, 0^{-})$ and $u_r^{(\mathrm{imp})}(x_1, h^{+}) - u_r^{(\mathrm{imp})}(x_1, h^{-})$ (over interfaces I and II).

As the micro-cracks are periodically distributed on $x_2 = 0$ and $x_2 = h$ as described in Section 2, the loads $\sigma_{r2}^{(\mathrm{ext})}(x_1, 0)$ and $\sigma_{r2}^{(\mathrm{ext})}(x_1, h)$ on the micro-cracks are assumed to be periodic functions of x_1 with period L. They may be chosen to be constant functions. With such periodic loads on the periodically distributed interfacial micro-cracks, u_k and σ_{kj} are periodic functions of x_1 with period L.

Thus, the boundary value problem is to solve the equilibrium equations in (3) for $u_k^{(\mathrm{imp})}$ subject to the interfacial conditions in (9). In addition to (9), it is required that $\sigma_{kj}^{(\mathrm{imp})} \to 0$ as $x_1^2 + x_2^2 \to \infty$.

Once the boundary value problem is solved, the effective stiffness coefficients $k_{r\mathrm{I}}$ and $k_{r\mathrm{II}}$ of the micro-cracked interfaces by averaging the crack-opening displacements and the external stress on the interfaces, that is, via the formulae:

$$\begin{aligned}
\frac{k_{1\mathrm{I}}}{L}\int_{a_{\mathrm{I}}^*}^{b_{\mathrm{I}}^*} \Delta u_{1\mathrm{I}}^{(\mathrm{imp})}(x_1)dx_1 &= \frac{1}{L}\int_0^L \sigma_{12}^{(\mathrm{ext})}(x_1, 0)dx_1,\\
\frac{k_{2\mathrm{I}}}{L}\int_{a_{\mathrm{I}}^*}^{b_{\mathrm{I}}^*} \Delta u_{2\mathrm{I}}^{(\mathrm{imp})}(x_1)dx_1 &= \frac{1}{L}\int_0^L \sigma_{22}^{(\mathrm{ext})}(x_1, 0)dx_1,\\
\frac{k_{1\mathrm{II}}}{L}\int_{a_{\mathrm{II}}^*}^{b_{\mathrm{II}}^*} \Delta u_{1\mathrm{II}}^{(\mathrm{imp})}(x_1)dx_1 &= \frac{1}{L}\int_0^L \sigma_{12}^{(\mathrm{ext})}(x_1, h)dx_1,\\
\frac{k_{2\mathrm{II}}}{L}\int_{a_{\mathrm{II}}^*}^{b_{\mathrm{II}}^*} \Delta u_{2\mathrm{II}}^{(\mathrm{imp})}(x_1)dx_1 &= \frac{1}{L}\int_0^L \sigma_{22}^{(\mathrm{ext})}(x_1, h)dx_1.
\end{aligned} \tag{10}$$

4 Hypersingular boundary integro-differential equations

To formulate the boundary value problem in Section 3 in terms of hypersingular boundary integral equations, the trimaterial in Fig. 1 is divided into two subdomains $x_2 > h/2$ and $x_2 < h/2$ along the artificial plane boundary $x_2 = h/2$. Each of the subdomains may be regarded as a bimaterial consisting of a thin elastic layer and an elastic half-space. The boundary integral equations in Clements (1981) together with the perfect interface Green's function given in Berger and Tewary (2001) and Chen and Ang (2014) for a bimaterial are used to obtain the hypersingular integral and integro-differential equations separately for each of the two subdomains. The analysis in Wang, Ang and Fan (2015) is closely followed here to derive the hypersingular boundary integral equations.

From the analysis on the lower subdomain $x_2 < h/2$, the stress $\sigma_{i2}^{(\mathrm{imp})}$ on the artificial boundary $x_2 = h^-/2$ is given by the hypersingular boundary integral equations

$$\begin{aligned}
&\pi\sigma_{i2}^{(\mathrm{imp})}(\xi_1, h^-/2)\\
&= \mathscr{H}\int_0^L u_r^{(imp)}\left(x_1, h^-/2\right) \mathrm{Re}\left\{\sum_{\alpha=1}^{2} G_{ri\alpha}\right\}\left[\frac{1}{(x_1-\xi_1)^2} + \Theta(x_1, \xi_1)\right] dx_1
\end{aligned}$$

$$+\int_0^L u_r^{(imp)}\left(x_1,h^-/2\right)\mathrm{Re}\left\{\sum_{\alpha=1}^{2}\sum_{\beta=1}^{2}H_{ri\alpha\beta\mathrm{I}}\Omega\left(x_1,\xi_1,\left(\tau_\alpha^{(2)}-\bar{\tau}_\beta^{(2)}\right)h^-/2\right)\right\}dx_1$$

$$+\mathscr{C}\int_0^L \sigma_{r2}^{(imp)}\left(x_1,h^-/2\right)\mathrm{Re}\left\{\sum_{\alpha=1}^{2}E_{ria}\right\}\left[\frac{1}{x_1-\xi_1}+\Lambda\left(x_1,\xi_1\right)\right]dx_1$$

$$+\int_0^L \sigma_{r2}^{(imp)}\left(x_1,h^-/2\right)\mathrm{Re}\left\{\sum_{\alpha=1}^{2}\sum_{\beta=1}^{2}F_{ri\alpha\beta\mathrm{I}}\Pi\left(x_1,\xi_1,\left(\tau_\alpha^{(2)}-\bar{\tau}_\beta^{(2)}\right)h^-/2\right)\right\}dx_1$$

$$-\int_{a_\mathrm{I}^*}^{b_\mathrm{I}^*}\Delta u_{r\mathrm{I}}^{(imp)}\left(x_1\right)\mathrm{Re}\left\{\sum_{\alpha=1}^{2}G_{ri\alpha}\Omega\left(x_1,\xi_1,-\tau_\alpha^{(2)}h^-/2\right)\right\}dx_1$$

$$-\int_{a_\mathrm{I}^*}^{b_\mathrm{I}^*}\Delta u_{r\mathrm{I}}^{(imp)}\left(x_1\right)\mathrm{Re}\left\{\sum_{\alpha=1}^{2}\sum_{\beta=1}^{2}H_{ri\alpha\beta\mathrm{I}}\Omega\left(x_1,\xi_1,-\bar{\tau}_\beta^{(2)}h^-/2\right)\right\}dx_1$$

$$\text{for } 0<\xi_1<L, \tag{11}$$

and the conditions on interface I, as given in (9), may be expressed in terms of the hypersingular boundary integro-differential equations

$$\int_0^L u_r^{(imp)}\left(x_1,h^-/2\right)\mathrm{Re}\left\{\sum_{\alpha=1}^{2}\Omega\left(x_1,\xi_1,\tau_\alpha^{(2)}h/2\right)\left(G_{ri\alpha}+\sum_{\beta=1}^{2}H_{ri\alpha\beta I}\right)\right\}dx_1$$

$$+\int_0^L (x_1,h^-/2)\mathrm{Re}\left\{\sum_{\alpha=1}^{2}\Pi(x_1,\xi_1,\tau_\alpha^{(2)}h^-/2)\left(E_{ri\alpha}+\sum_{\beta=1}^{2}F_{ri\alpha\beta\mathrm{I}}\right)\right\}dx_1$$

$$-\mathscr{H}\int_{a_\mathrm{I}^*}^{b_\mathrm{I}^*}\frac{\Delta u_{r\mathrm{I}}(x_1)\mathrm{Re}\{W_{ri\mathrm{I}}\}}{(x_1-\xi_1)^2}dx_1 \tag{12}$$

$$-\int_{a_\mathrm{I}^*}^{b_\mathrm{I}^*}\Delta u_{r\mathrm{I}}(x_1)\mathrm{Re}\{W_{ri\mathrm{I}}\}\Theta(x_1,\xi_1)dx_1+\mathrm{Im}\{\pi V_{ri\mathrm{I}}\}\frac{d}{d\xi_1}[\Delta u_{r\mathrm{I}}(\xi_1)]$$

$$=-2\pi\sigma_{i2}^{(\mathrm{ext})}(\xi_1,0^+)\text{ for }a_\mathrm{I}^*<\xi_1<b_\mathrm{I}^*, \tag{13}$$

where $\mathscr{C}$ and $\mathscr{H}$ denote that the integral is to be interpreted in the Cauchy principal and the Hadamard finite-part sense respectively, Re denotes the real part of a complex number, the overhead bar denotes the complex conjugate of a complex number, the constants $G_{ri\alpha}$, $H_{ri\alpha\beta\mathrm{I}}$, $W_{ri\mathrm{I}}$, $V_{ri\mathrm{I}}$, $E_{ri\alpha}$ and $F_{ri\alpha\beta\mathrm{I}}$ are defined by

$$G_{ri\alpha}=\left[L_{r2\alpha}^{(2)}N_{\alpha p}^{(2)}\left(C_{i2m1}^{(2)}+\tau_\alpha^{(2)}C_{i2m2}^{(2)}\right)\right]D_{pm}^{(2)},$$

$$H_{ri\alpha\beta\mathrm{I}}=\left[L_{r2\alpha}^{(2)}Q_{\alpha\beta p}^{(2)}\left(C_{i2m1}^{(2)}+\bar{\tau}_\beta^{(2)}C_{i2m2}^{(2)}\right)\right]D_{pm}^{(2)},$$

$$W_{ri\mathrm{I}}=\sum_{\alpha=1}^{2}G_{ri\alpha}+\sum_{\alpha=1}^{2}\sum_{\beta=1}^{2}H_{ri\alpha\beta\mathrm{I}},$$

$$V_{ri\mathrm{I}} = \sum_{\alpha=1}^{2}\sum_{\beta=1}^{2} H_{ri\alpha\beta\mathrm{I}} - \sum_{\alpha=1}^{2} G_{ri\alpha},$$
$$E_{ri\alpha} = \left[A_{r\alpha}^{(2)} N_{\alpha p}^{(2)} \left(C_{i2m1}^{(2)} + \tau_{\alpha}^{(2)} C_{i2m2}^{(2)}\right)\right] D_{pm}^{(2)},$$
$$F_{ri\alpha\beta\mathrm{I}} = \left[A_{r\alpha}^{(2)} Q_{\alpha\beta p}^{(2)} \left(C_{i2m1}^{(2)} + \overline{\tau}_{\beta}^{(2)} C_{i2m2}^{(2)}\right)\right] D_{pm}^{(2)},$$

the constants $A_{m\alpha}^{(q)}$ are given by

$$\left[A_{m\alpha}^{(q)}\right] = \begin{bmatrix} -\dfrac{i\tau_1^{(q)}\left[C_{12}^{(q)} + C_{66}^{(q)}\right]}{C_{11}^{(q)} + C_{66}^{(q)}(\tau_1^{(q)})^2} & -\dfrac{i\tau_2^{(q)}\left[C_{12}^{(q)} + C_{66}^{(q)}\right]}{C_{11}^{(q)} + C_{66}^{(q)}\left(\tau_2^{(q)}\right)^2} \\ i & i \end{bmatrix},$$

$i = \sqrt{-1}$, $L_{i2\alpha}^{(q)}$ are given by

$$L_{12\alpha}^{(q)} = C_{66}^{(q)}\left(\tau_{\alpha}^{(q)} A_{1\alpha}^{(q)} + A_{2\alpha}^{(q)}\right),$$
$$L_{22\alpha}^{(q)} = C_{12}^{(q)} A_{1\alpha}^{(q)} + \tau_{\alpha}^{(q)} C_{22}^{(q)} A_{2\alpha}^{(q)},$$

the constants $\tau_1^{(q)}$ and $\tau_2^{(q)}$ are two distinct complex numbers with positive imaginary parts and are solutions of the quartic equation in τ given by

$$C_{22}^{(q)} C_{66}^{(q)} \tau^4 - ([C_{12}^{(q)}]^2 + 2C_{12}^{(q)} C_{66}^{(q)} - C_{22}^{(q)} C_{11}^{(q)})\tau^2 + C_{11}^{(q)} C_{66}^{(q)} = 0, \tag{14}$$

the matrices $[N_{\alpha p}^{(q)}]$ and $[M_{\alpha p}^{(q)}]$ are the inverses of $[A_{k\alpha}^{(q)}]$ and $[L_{k2\alpha}^{(q)}]$ respectively, the constants $D_{rp}^{(q)}$ are defined implicitly by

$$\mathrm{Im}\left\{\sum_{\alpha=1}^{2} L_{i2\alpha}^{(q)} N_{\alpha r}^{(q)}\right\} D_{rp}^{(q)} = \delta_{ip}, \tag{15}$$

δ_{ip} is Kronecker-delta, Im denotes the imaginary part of a complex number, the constants $Q_{\alpha\beta p}^{(2)}$ are implicitly defined by (see Chen and Ang (2014))

$$\sum_{\alpha=1}^{2}\left[N_{\gamma r}^{(3)} \overline{A}_{r\alpha}^{(2)} - M_{\gamma r}^{(3)} \overline{L}_{r2\alpha}^{(2)}\right] \overline{Q}_{\alpha\beta p}^{(2)} = \left[M_{\gamma r}^{(3)} L_{r2\beta}^{(2)} - N_{\gamma r}^{(3)} A_{r\beta}^{(2)}\right] N_{\beta p}^{(2)}, \tag{16}$$

and the functions $\Lambda(x_1, \xi_1), \Pi(x_1, \xi_1, z), \Theta(x_1, \xi_1)$ and $\Omega(x_1, \xi_1, z)$ are defined by

$$\Lambda(x_1, \xi_1) = \frac{1}{L}\Psi\left(\frac{L - x_1 + \xi_1}{L}\right) - \frac{1}{L}\Psi\left(\frac{L + x_1 - \xi_1}{L}\right),$$

$$\Pi(x_1,\xi_1,z)=\frac{1}{x_1-\xi_1+z}+\frac{1}{L}\Psi\left(\frac{L-x_1+\xi_1-z}{L}\right)-\frac{1}{L}\Psi\left(\frac{L+x_1-\xi_1+z}{L}\right),$$

$$\Theta(x_1,\xi_1)=\frac{1}{L^2}\Psi_1\left(\frac{L+x_1-\xi_1}{L}\right)+\frac{1}{L^2}\Psi_1\left(\frac{L+\xi_1-x_1}{L}\right),$$

$$\Omega(x_1,\xi_1,z)=\frac{1}{(x_1-\xi_1+z)^2}+\frac{1}{L^2}\Psi_1\left(\frac{L+x_1-\xi_1+z}{L}\right)+\frac{1}{L^2}\Psi_1\left(\frac{L-x_1+\xi_1-z}{L}\right),$$

with $\Psi(z)$ and $\Psi_1(z)$ being the digamma and trigamma functions respectively (see Abramowitz and Stegun (1970)). Note that the usual Einsteinian convention of summing over a repeated index is applicable here only for lowercase Latin subscripts from 1 to 2.

Similarly, from the analysis on the upper subdomain $x_2 > h/2$, the stress $\sigma_{i2}^{(\mathrm{imp})}$ on the artificial boundary $x_2 = h^+/2$ is given by the hypersingular boundary integral equations

$$\begin{aligned}
&\pi\sigma_{i2}^{(\mathrm{imp})}(\xi_1,h^+/2)\\
&=-\mathscr{H}\int_0^L u_r^{(\mathrm{imp})}(x_1,h^+/2)\mathrm{Re}\left\{\sum_{\alpha=1}^{2}G_{ri\alpha}\right\}\left[\frac{1}{(x_1-\xi_1)^2}+\Theta(x_1,\xi_1)\right]dx_1\\
&\quad-\int_0^L u_r^{(\mathrm{imp})}(x_1,h^+/2)\mathrm{Re}\left\{\sum_{\alpha=1}^{2}\sum_{\beta=1}^{2}H_{ri\alpha\beta\mathrm{II}}\Omega\left(x_1,\xi_1,-\left(\tau_\alpha^{(2)}-\overline{\tau}_\beta^{(2)}\right)h/2\right)\right\}dx_1\\
&\quad-\mathscr{C}\int_0^L \sigma_{r2}^{(\mathrm{imp})}(x_1,h^+/2)\mathrm{Re}\left\{\sum_{\alpha=1}^{2}E_{ri\alpha}\right\}\left[\frac{1}{x_1-\xi_1}+\Lambda(x_1,\xi_1)\right]dx_1\\
&\quad-\int_0^L \sigma_{r2}^{(\mathrm{imp})}(x_1,h^+/2)\mathrm{Re}\left\{\sum_{\alpha=1}^{2}\sum_{\beta=1}^{2}F_{ri\alpha\beta\mathrm{II}}\Pi\left(x_1,\xi_1,-\left(\tau_\alpha^{(2)}-\overline{\tau}_\beta^{(2)}\right)h/2\right)\right\}dx_1\\
&\quad-\int_{a_{\mathrm{II}}^*}^{b_{\mathrm{II}}^*}\Delta u_{r\mathrm{II}}^{(\mathrm{imp})}(x_1)\mathrm{Re}\left\{\sum_{\alpha=1}^{2}G_{ri\alpha}\Omega\left(x_1,\xi_1,\tau_\alpha^{(2)}h/2\right)\right\}dx_1\\
&\quad-\int_{a_{\mathrm{II}}^*}^{b_{\mathrm{II}}^*}\Delta u_{r\mathrm{II}}^{(\mathrm{imp})}(x_1)\mathrm{Re}\left\{\sum_{\alpha=1}^{2}\sum_{\beta=1}^{2}H_{ri\alpha\beta\mathrm{II}}\Omega\left(x_1,\xi_1,\overline{\tau}_\beta^{(2)}h/2\right)\right\}dx_1\\
&\quad\text{for } 0<\xi_1<L,
\end{aligned}\tag{17}$$

and the conditions on interface II may be expressed in terms of the hypersingular

boundary integro-differential equations

$$\int_0^L u_r^{(\mathrm{imp})}\left(x_1,h^+/2\right)\mathrm{Re}\left\{\sum_{\alpha=1}^{2}\Omega\left(x_1,\xi_1,-\tau_\alpha^{(2)}h^-/2\right)\left(G_{ri\alpha}+\sum_{\beta=1}^{2}H_{ri\alpha\beta\mathrm{II}}\right)\right\}dx_1$$
$$+\int_0^L \sigma_{r2}^{(\mathrm{imp})}(x_1,h^+/2)\mathrm{Re}\left\{\sum_{\alpha=1}^{2}\Pi(x_1,\xi_1,-\tau_\alpha^{(2)}h^-/2)\left(E_{ri\alpha}+\sum_{\beta=1}^{2}F_{ri\alpha\beta\mathrm{II}}\right)\right\}dx_1$$
$$+\mathscr{H}\int_{a_{\mathrm{II}}^*}^{b_{\mathrm{II}}^*}\frac{\Delta u_{r\mathrm{II}}(x_1)\mathrm{Re}\{W_{ri\mathrm{II}}\}}{(x_1-\xi_1)^2}dx_1$$
$$+\int_{a_{\mathrm{II}}^*}^{b_{\mathrm{II}}^*}\Delta u_{r\mathrm{II}}(x_1)Re\{W_{ri\mathrm{II}}\}\Theta(x_1,\xi_1)dx_1+\frac{d\Delta u_{r\mathrm{II}}(\xi_1)}{d\xi_1}\mathrm{Im}\{\pi V_{ri\mathrm{II}}\}$$
$$=2\pi\sigma_{i2}^{(\mathrm{ext})}(\xi_1,h^-)\text{ for }a_{\mathrm{II}}^*<\xi_1<b_{\mathrm{II}}^*, \tag{18}$$

where $H_{ri\alpha\beta\mathrm{II}}$, $F_{ri\alpha\beta\mathrm{II}}$, $W_{ri\mathrm{II}}$ and $V_{ri\mathrm{II}}$ are given by

$$H_{ri\alpha\beta\mathrm{II}}=\left[L_{r2\alpha}^{(2)}T_{\alpha\beta p}^{(2)}\left(C_{i2m1}^{(2)}+\overline{\tau}_\beta^{(2)}C_{i2m2}^{(2)}\right)\right]D_{pm}^{(2)},$$
$$F_{ri\alpha\beta\mathrm{II}}=\left[A_{r\alpha}^{(2)}T_{\alpha\beta p}^{(2)}\left(C_{i2m1}^{(2)}+\overline{\tau}_\beta^{(2)}C_{i2m2}^{(2)}\right)\right]D_{pm}^{(2)},$$
$$W_{ri\mathrm{II}}=\sum_{\alpha=1}^{2}G_{ri\alpha}+\sum_{\alpha=1}^{2}\sum_{\beta=1}^{2}H_{ri\alpha\beta\mathrm{II}},$$
$$V_{ri\mathrm{II}}=\sum_{\alpha=1}^{2}\sum_{\beta=1}^{2}H_{ri\alpha\beta\mathrm{II}}-\sum_{\alpha=1}^{2}G_{ri\alpha},$$

and the constants $T_{\alpha\beta p}^{(2)}$ may be implicitly defined by

$$\sum_{\alpha=1}^{2}\left[N_{\gamma k}^{(1)}\overline{A}_{k\alpha}^{(2)}-M_{\gamma k}^{(1)}\overline{L}_{k2\alpha}^{(2)}\right]\overline{T}_{\alpha\beta p}^{(2)}=\left[M_{\gamma k}^{(1)}L_{k2\beta}^{(2)}-N_{\gamma k}^{(1)}A_{k\beta}^{(2)}\right]N_{\beta p}^{(2)}. \tag{19}$$

Note that (11), (12), (16) and (17) do not contain any integral over the perfect (uncracked) parts of interfaces I and II because of the use of the special perfect interface Green's function given in Berger and Tewary (2001) and Chen and Ang (2014).

In (11), (12), (16) and (17), there are 12 unknown functions given by the displacements $u_r^{(\mathrm{imp})}(x_1,h^+/2), u_r^{(\mathrm{imp})}(x_1,h^-/2)$, the stresses $\sigma_{r2}^{(\mathrm{imp})}(x_1,h^+/2), \sigma_{r2}^{(\mathrm{imp})}(x_1,h^-/2)$ and the crack opening displacements $\Delta u_{r\mathrm{I}}^{(\mathrm{imp})}(x_1)$ and $\Delta u_{r\mathrm{II}}^{(\mathrm{imp})}(x_1)$ on interfaces I and II respectively. However, there are only 8 equations in (11), (12), (16)

and (17). Four more equations are required to complete the formulation. They are given by the continuity conditions on the artificial boundary $x_2 = h/2$ as follows:

$$\left.\begin{aligned} u_r^{(\mathrm{imp})}(x_1, h^+/2) &= u_r^{(\mathrm{imp})}(x_1, h^-/2) \\ \sigma_{r2}^{(\mathrm{imp})}(x_1, h^+/2) &= \sigma_{r2}^{(\mathrm{imp})}(x_1, h^-/2) \end{aligned}\right\} \text{ for } -\infty < x_1 < \infty, r = 1,2. \tag{20}$$

Once $\Delta u_{r\mathrm{I}}^{(\mathrm{imp})}(x_1)$ and $\Delta u_{r\mathrm{II}}^{(\mathrm{imp})}(x_1)$ are determined by solving (11), (12), (16) and (17) together with (19), the effective stiffness coefficients $k_{r\mathrm{I}}$ and $k_{r\mathrm{II}}$ for interfaces I and II respectively may be estimated by using (10).

5 Numerical procedure

The numerical procedure for solving the hypersingular integral and integro-differential equations (11), (12), (16) and (17) together with (19) is outlined below.

The part of the artificial boundary $x_2 = h/2$ where $0 \le x_1 \le L$ is discretized into N_t equal subintervals given by

$$x_t^{(p)} \le x_1 \le x_t^{(p+1)}, x_2 = h/2 (p = 1,2,\ldots,N_t).$$

The unknown functions $u_r^{(\mathrm{imp})}(x_1, h^{\pm}/2)$ and $\sigma_{r2}^{(\mathrm{imp})}(x_1, h^{\pm}/2)$ are approximated over the p-th subinterval

$$\left.\begin{aligned} u_r^{(\mathrm{imp})}(x_1, h^{\pm}/2) &\approx x_1 \phi_r^{(p)} + \psi_r^{(p)} \\ \sigma_{r2}^{(\mathrm{imp})}(x_1, h^{\pm}/2) &\approx x_1 \vartheta_r^{(p)} + \eta_r^{(p)} \end{aligned}\right\} \text{ for } x_t^{(p)} \le x_1 \le x_t^{(p+1)}, \tag{21}$$

where $\phi_r^{(p)}, \psi_r^{(p)}, \vartheta_r^{(p)}$ and $\eta_r^{(p)}$ are $8N_t$ constants yet to be determined.

To generate $8N_t$ equations, the hypersingular integral equations (11) and (16) may be collocated at two points per subinterval over the region where $0 < x_1 < L$, $x_2 = h/2$. The two collocations points on the p-th subinterval are chosen to be

$$\left.\begin{aligned} (\tilde{x}_t^{(p)}, h/2) &= \left(\frac{3}{4}x_t^{(p)} + \frac{1}{4}x_t^{(p+1)}, h/2\right) \\ (\tilde{x}_t^{(p+N_t)}, h/2) &= \left(\frac{1}{4}x_t^{(p)} + \frac{3}{4}x_t^{(p+1)}, h/2\right) \end{aligned}\right\} \text{ for } p = 1,2,\ldots,N_t, \tag{22}$$

As in Kaya and Erdogan (1987), the unknown crack opening displacements $\Delta u_{r\mathrm{I}}^{(\mathrm{imp})}(x_1)$ and $\Delta u_{r\mathrm{II}}^{(\mathrm{imp})}(x_1)$ on interfaces I and II respectively may be approximated by using

$$\Delta u_{r\mathrm{I}}^{(\mathrm{imp})}(x_1) \approx \sqrt{(x_1 - a_{\mathrm{I}}^*)(b_{\mathrm{I}}^* - x_1)} \times \sum_{m=1}^{N_{\mathrm{cI}}} \alpha_{r\mathrm{I}}^{(m)} U^{(m-1)}\left(\frac{2x_1 - b_{\mathrm{I}}^* - a_{\mathrm{I}}^*}{b_{\mathrm{I}}^* - a_{\mathrm{I}}^*}\right) \tag{23}$$

for $a_{\mathrm{I}}^* < x_1 < b_{\mathrm{I}}^*$,

and

$$\Delta u_{r\mathrm{II}}^{(\mathrm{imp})}(x_1) \approx \sqrt{(x_1-a_{\mathrm{II}}^*)(b_{\mathrm{II}}^*-x_1)} \times \sum_{m=1}^{N_{\mathrm{cII}}} \alpha_{r\mathrm{II}}^{(m)} U^{(m-1)}\left(\frac{2x_1-b_{\mathrm{II}}^*-a_{\mathrm{II}}^*}{b_{\mathrm{II}}^*-a_{\mathrm{II}}^*}\right) \tag{24}$$

for $a_{\mathrm{II}}^* < x_1 < b_{\mathrm{II}}^*$,

where $\alpha_{r\mathrm{I}}^{(m)}$ and $\alpha_{r\mathrm{II}}^{(m)}$ are $N_{\mathrm{cI}}+N_{\mathrm{cII}}$ constants yet to be determined, N_{cI} and N_{cII} are positive integers and $U^{(m)}(x_1)$ is the m-th order Chebyshev polynomial of the second kind.

The hypersingular integro-differential equations (12) and (17) may be collocated at N_{cI} and N_{cII} points respectively to generate $N_{\mathrm{cI}}+N_{\mathrm{cII}}$ equations. The collocation points over $a_{\mathrm{I}}^* < x_1 < b_{\mathrm{I}}^*$ are chosen to be given by

$$\left(x_{\mathrm{cI}}^{(m)},0\right) = \left(\frac{a_{\mathrm{I}}^*+b_{\mathrm{I}}^*}{2} + \frac{b_{\mathrm{I}}^*-a_{\mathrm{I}}^*}{2}\cos\left(\frac{[2m-1]\pi}{2N_{\mathrm{cI}}}\right),0\right) \quad \text{for } m=1,2,\cdots,N_{\mathrm{cI}}, \tag{25}$$

and those over $a_{\mathrm{II}}^* < x_1 < b_{\mathrm{II}}^*$ by

$$\left(x_{\mathrm{cII}}^{(m)},h\right) = \left(\frac{a_{\mathrm{II}}^*+b_{\mathrm{II}}^*}{2} + \frac{b_{\mathrm{II}}^*-a_{\mathrm{II}}^*}{2}\cos\left(\frac{[2m-1]\pi}{2N_{\mathrm{cII}}}\right),h\right) \quad \text{for } m=1,2,\cdots,N_{\mathrm{cII}}. \tag{26}$$

If the approximations in (20), (22) and (23) are substituted into hypersingular boundary integro-differential equations (11), (12), (16) and (17) collocated at the relevant collocation points defined by (21), (24) and (25) and if the continuity conditions (19) is used, a system of linear algebraic equations may be set up to determine the $8N_t+N_{\mathrm{cI}}+N_{\mathrm{cII}}$ unknown constants in (20), (22) and (23). Once $\alpha_{r\mathrm{I}}^{(m)}$ and $\alpha_{r\mathrm{II}}^{(m)}$ are obtained, the effective stiffness coefficients $k_{r\mathrm{I}}$ and $k_{r\mathrm{II}}$ may be easily computed by substituting (22) and (23) into (10).

6 Specific cases

Some specific cases of the problem are examined here by using particular orthotropic materials. The materials and their elastic moduli (in GPa) (taken from Glodež and Jezernik (2010), Guechaichia and Trendafilova (2012) and Rubio-Gonzalez and Mason (2000)) are given in Tab. 1.

Case (a): The interface II is taken to be perfect, that is, $\rho_{\mathrm{II}}=0$. The materials in the layer and the lower half-space are carbon-epoxy and graphite-epoxy respectively. The elastic moduli (in GPa) of the material in the upper half-space are chosen to be

$$C_{11}^{(1)} = 136.2\alpha, C_{22}^{(1)} = 9.2\alpha, C_{12}^{(1)} = 3.9\alpha, C_{66}^{(1)} = 4.3\alpha,$$

Table 1: Elastic moduli (in GPa) for selected orthotropic materials.

Material	C_{11}	C_{22}	C_{12}	C_{66}
Carbon-epoxy	136.2	9.2	3.9	4.3
E-glass-epoxy	46.1	12.6	2.9	5.5
Graphite-epoxy	155.4	16.3	3.7	7.5
Martensite	233.0	233.0	135.0	188.0

where α is a positive constant.

If α is very small, the material in the upper half-space is extremely soft compared to the materials in the layer and the lower half-space. Thus, the limiting case in which $\alpha \to 0^+$ gives a micro-cracked interface between an elastic half-space and a thin layer with one of its edges acted upon by prescribed tractions, as considered in Wang, Ang and Fan (2015).

If $\alpha = 1$, the upper half-space and the layer are both occupied by carbon-epoxy. Since the interface II is perfect, $\alpha = 1$ corresponds to the special case of a micro-cracked interface (given by interface I) between two dissimilar homogeneous elastic half-spaces. Such a special case can also be recovered from the analysis here for any other value of α by letting the width of the layer tend to infinity.

For $\rho_{\rm I} = 0.5$, the non-dimensionalized effective stiffness coefficients $a_{\rm I}k_{1\rm I}/C_{66}^{(2)}$ and $a_{\rm I}k_{2\rm I}/C_{66}^{(2)}$ are plotted against $a_{\rm I}/h$ for selected values of α. The graphs of $a_{\rm I}k_{1\rm I}/C_{66}^{(2)}$ and $a_{\rm I}k_{2\rm I}/C_{66}^{(2)}$ for the special case $\alpha \to 0^+$, obtained by using the analysis Wang, Ang and Fan (2015), are also given in Fig. 2. It is obvious that the graphs of $a_{\rm I}k_{1\rm I}/C_{66}^{(2)}$ and $a_{\rm I}k_{2\rm I}/C_{66}^{(2)}$ for smaller values of α are closer to those for $\alpha \to 0^+$. This gives a check for the analysis here against the one in Wang, Ang and Fan (2015).

As expected, the values of $a_{\rm I}k_{1\rm I}/C_{66}^{(2)}$ and $a_{\rm I}k_{2\rm I}/C_{66}^{(2)}$ for $\alpha = 1$ are constants independent of $a_{\rm I}/h$. As noted earlier on, the case $\alpha = 1$ can also be recovered from the analysis here for other values of α by letting the width of the layer tend to infinity. This is why Fig. 2 shows that the graphs of $a_{\rm I}k_{1\rm I}/C_{66}^{(2)}$ and $a_{\rm I}k_{2\rm I}/C_{66}^{(2)}$ converge to the constant values of the effective stiffness coefficients for $\alpha = 1$ as $a_{\rm I}/h$ approaches 0^+.

For a fixed α, the non-dimensionalized effective stiffness coefficients $a_{\rm I}k_{1\rm I}/C_{66}^{(2)}$ and $a_{\rm I}k_{2\rm I}/C_{66}^{(2)}$ in Fig. 2 are observed to decrease and increase as $a_{\rm I}/h$ increases for $\alpha < 1$ and $\alpha > 1$ respectively. This observation may be explained as follows. The perfectly bonded thin layer and the upper half-space may be considered as a "combined half-space". For $\alpha < 1$, the upper half-space is softer than the thin layer. Thus, the "combined half-space" becomes softer as the thin layer width decreases

(that is, as a_{I}/h increases), giving larger average values of $\Delta u_{r\mathrm{I}}^{(\mathrm{imp})}(x_1)$ over interface I for larger a_{I}/h. For $\alpha > 1$, the upper half-space is harder than the thin layer and hence the average values of $\Delta u_{r\mathrm{I}}^{(\mathrm{imp})}(x_1)$ over interface I are smaller for larger a_{I}/h.

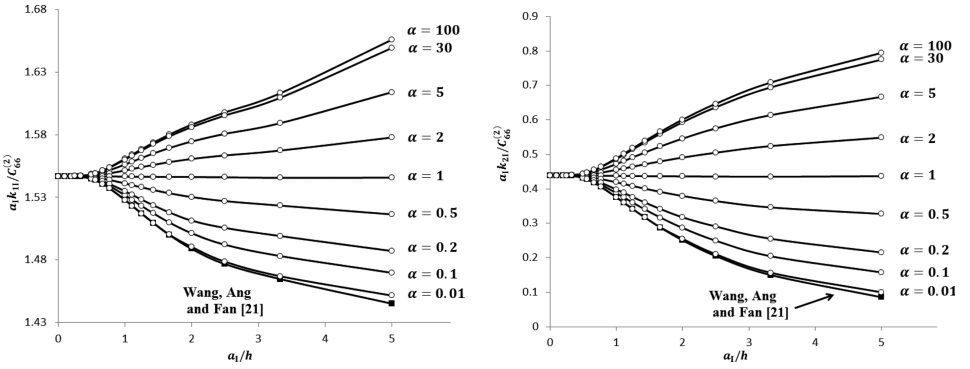

Figure 2: Plots of $a_{\mathrm{I}}k_{1\mathrm{I}}/C_{66}^{(2)}$ and $a_{\mathrm{I}}k_{2\mathrm{I}}/C_{66}^{(2)}$ against a_{I}/h for the cases where interface II is perfectly bonded with $\rho_{\mathrm{I}} = 0.5$ and selected values of α

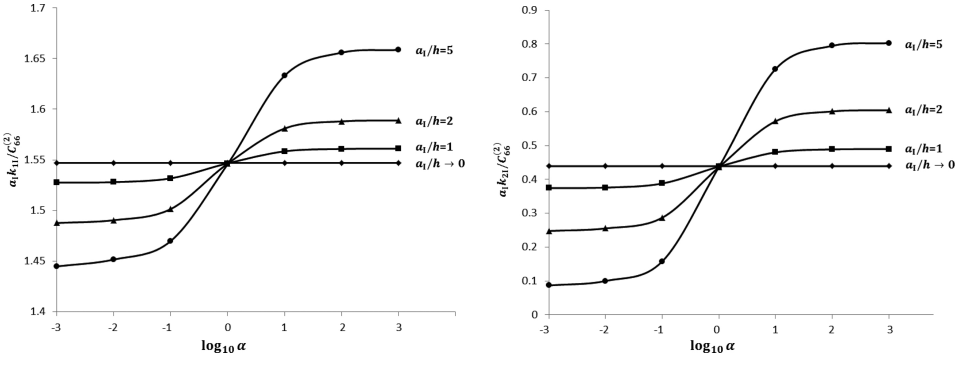

Figure 3: Plots of $a_{\mathrm{I}}k_{1\mathrm{I}}/C_{66}^{(2)}$ and $a_{\mathrm{I}}k_{2\mathrm{I}}/C_{66}^{(2)}$ against $\log_{10}\alpha$ for the cases where interface II is perfectly bonded with $\rho_{\mathrm{I}} = 0.5$ and selected values of α

For a fixed value of a_{I}/h, Fig. 2 shows that $a_{\mathrm{I}}k_{1\mathrm{I}}/C_{66}^{(2)}$ and $a_{\mathrm{I}}k_{2\mathrm{I}}/C_{66}^{(2)}$ become larger as α increases. For the limiting case in which $\alpha \to \infty$, the layer is perfectly bonded to a rigid wall along the plane $x_2 = h$ (so that $u_1 = u_2 = 0$ on $x_2 = h$). It may be of some interest to examine in details how $a_{\mathrm{I}}k_{1\mathrm{I}}/C_{66}^{(2)}$ and $a_{\mathrm{I}}k_{2\mathrm{I}}/C_{66}^{(2)}$ vary with α for

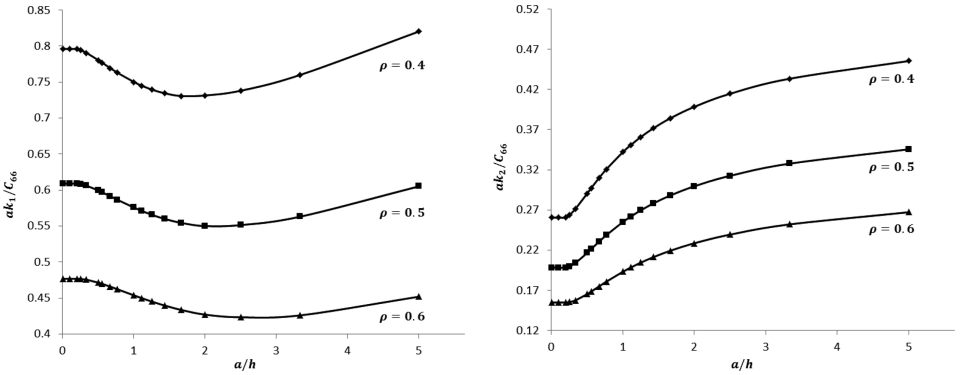

(a) (b)

Figure 4: Plots of ak_1/C_{66} and ak_2/C_{66} against a/h for $\rho = 0.4, 0.5$ and 0.6

a fixed value of a_{I}/h. For $\rho_{\mathrm{I}} = 0.5$, Fig. 3 plots $a_{\mathrm{I}}k_{1\mathrm{I}}/C_{66}^{(2)}$ and $a_{\mathrm{I}}k_{2\mathrm{I}}/C_{66}^{(2)}$ against $\log_{10}\alpha$ for selected values of a_{I}/h. From the graphs for a given a_{I}/h, it is apparent that $a_{\mathrm{I}}k_{1\mathrm{I}}/C_{66}^{(2)}$ and $a_{\mathrm{I}}k_{2\mathrm{I}}/C_{66}^{(2)}$ tend to some constant values as $\alpha \to \infty$.

Case (b): The thin layer and the two half-spaces are occupied by the same orthotropic material. The material is taken to be graphite-epoxy. The interfaces are taken to be identical, so that $\rho_{\mathrm{I}} = \rho_{\mathrm{II}} = \rho$, hence $a_{\mathrm{I}} = a_{\mathrm{II}} = a$, where a and ρ are constants such that $\rho = 2a/L$. For such a case, the effective stiffness coefficients are such that $k_{1\mathrm{I}} = k_{1\mathrm{II}} = k_1$ and $k_{2\mathrm{I}} = k_{2\mathrm{II}} = k_2$.

In Fig. 4, the non-dimensionalized effective stiffness coefficients ak_1/C_{66} and ak_2/C_{66} are plotted against a/h for selected values of ρ. Note that $C_{66} = 7.5$ GPa for graphite epoxy. For a given value of ρ, non-dimensionalized effective stiffness coefficient ak_1/C_{66} is observed to have a local minimum at a certain value of a/h. The value of a/h where the local minimum of ak_1/C_{66} occurs appears to increase with ρ.

Also, for a given ρ, the non-dimensionalized effective stiffness coefficient ak_2/C_{66} appears to increase as a/h increases. This may be explained by taking into consideration the crack shielding effect described in Gao, Lee and Zhou (2012), that is, for two parallel cracks in a homogeneous elastic space under remote pure tensile load, the crack opening displacement $\Delta u_2^{(\mathrm{imp})}(x_1)$ of each of the cracks decreases as the cracks gets closer to each other.

For a given value of a/h, it appears that ak_1/C_{66} and ak_2/C_{66} have larger values for smaller values of ρ. This is not surprising as the micro-cracks are more stable and have smaller crack opening displacements if the micro-cracks have lower density on the interfaces.

Case (c): As in Case (b), the layer and the half-spaces are occupied by graphite-epoxy. However, $\rho_{\rm I}$ and $\rho_{\rm II}$ are not necessarily equal here. For such a case, it may be more instructive to non-dimensionalize the effective stiffness coefficients as $(a_{\rm I}+a_{\rm II})k_{r\rm I}/(2C_{66})$ and $(a_{\rm I}+a_{\rm II})k_{r\rm II}/(2C_{66})$.

For $\rho_{\rm I}=0.5$, the non-dimensionalized effective stiffness coefficients $(a_{\rm I}+a_{\rm II})k_{r\rm I}/(2C_{66})$ and $(a_{\rm I}+a_{\rm II})k_{r\rm II}/(2C_{66})$ are plotted against $(a_{\rm I}+a_{\rm II})/(2h)$ for selected values of $\rho_{\rm II}$ in Figs. 5 and 6 respectively. As expected, Figs. 5 and 6 show that the graph of $(a_{\rm I}+a_{\rm II})k_{r\rm I}/(2C_{66})$ is the same as that of $(a_{\rm I}+a_{\rm II})k_{r\rm II}/(2C_{66})$ for $\rho_{\rm II}=0.5$ (that is, when interfaces I and II have the same damage ratio). For $\rho_{\rm I}=0.5$ and given values of $\rho_{\rm II}$ and $(a_{\rm I}+a_{\rm II})/(2h)$, Figs. 5 and 6 show that $k_{r\rm I}<k_{r\rm II}$ for $\rho_{\rm II}<0.5$ and $k_{r\rm I}>k_{r\rm II}$ for $\rho_{\rm II}>0.5$. This observation is as expected because of the following reason. For $\rho_{\rm II}<0.5$, interface II is less severely damaged than interface I ($\rho_{\rm I}=0.5$), hence $|\Delta u_{r\rm II}^{(\rm imp)}(x_1)|$ may be expected to be less than $|\Delta u_{r\rm I}^{(\rm imp)}(x_1)|$ to give $k_{r\rm II}>k_{r\rm I}$. Similarly, for $\rho_{\rm II}>0.5$, with interface II more severely damaged, $|\Delta u_{r\rm II}^{(\rm imp)}(x_1)|$ is greater than $|\Delta u_{r\rm I}^{(\rm imp)}(x_1)|$, hence $k_{r\rm II}<k_{r\rm I}$.

In Fig. 5, the range of values which the non-dimensionalized effective stiffness coefficients $(a_{\rm I}+a_{\rm II})k_{1\rm I}/(2C_{66})$ and $(a_{\rm I}+a_{\rm II})k_{2\rm I}/(2C_{66})$ (for interface I) can have over the interval $0<(a_{\rm I}+a_{\rm II})/(2h)\le 5$ is narrower if $\rho_{\rm II}$ has a smaller value. Thus, one may expect $(a_{\rm I}+a_{\rm II})k_{1\rm I}/(2C_{66})$ and $(a_{\rm I}+a_{\rm II})k_{2\rm I}/(2C_{66})$ to tend to parameters that are independent of $(a_{\rm I}+a_{\rm II})/(2h)$ as $\rho_{\rm II}\to 0$. This observation is consistent with the fact that the effective stiffness coefficients of interface II are independent of the width of the layer if interface II is perfect ($\rho_{\rm II}=0$) and the layer and the upper half-space are occupied by the same material.

For $\rho_{\rm I}=0.5$ and a given value of $(a_{\rm I}+a_{\rm II})/(2h)$, Fig. 6 shows that the values of $(a_{\rm I}+a_{\rm II})k_{1\rm II}/(2C_{66})$ and $(a_{\rm I}+a_{\rm II})k_{2\rm II}/(2C_{66})$ increase as $\rho_{\rm II}$ decreases to zero. This is as expected since both $k_{1\rm II}$ and $k_{2\rm II}$ should tend to infinity as $\rho_{\rm II}$ tends to zero, that is as interface II approaches being perfect. From Fig. 6, it is also apparent that $(a_{\rm I}+a_{\rm II})k_{2\rm II}/(2C_{66})$ increases with $(a_{\rm I}+a_{\rm II})/(2h)$ at a faster rate for a smaller value of $\rho_{\rm II}$.

Case (d): The thin layer is occupied by graphite-epoxy. The material in the upper half-space is taken to be the same as that in the lower half-space. One of the following materials — martensite, graphite-epoxy and e-glass-epoxy — is selected to occupy the half-spaces. As in Case (a) above, the interfaces are such that $\rho_{\rm I}=\rho_{\rm II}=\rho$ and $a_{\rm I}=a_{\rm II}=a$, hence $k_{1\rm I}=k_{1\rm II}=k_1$ and $k_{2\rm I}=k_{2\rm II}=k_2$.

For $\rho=0.5$, Fig. 7 plots the non-dimensionalized effective stiffness coefficients $ak_1/C_{66}^{(2)}$ and $ak_2/C_{66}^{(2)}$ against a/h for selected materials in the half-spaces. Note that the thin layer and the half-spaces are occupied by the same materials if the elastic moduli of graphite-epoxy are used for the half-spaces. Fig. 7(a) shows that, as

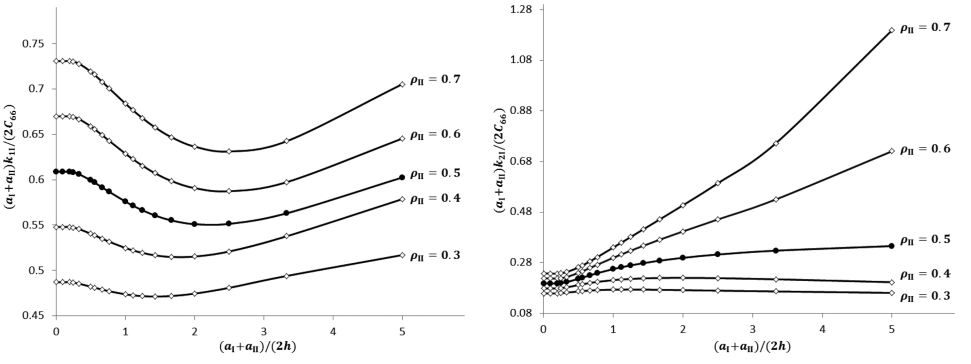

(a) (b)

Figure 5: Plots of $(a_I + a_{II})k_{1I}/(2C_{66}^{(2)})$ and $(a_I + a_{II})k_{2I}/(2C_{66}^{(2)})$ against $(a_I + a_{II})/(2h)$ for selected values of ρ_{II}

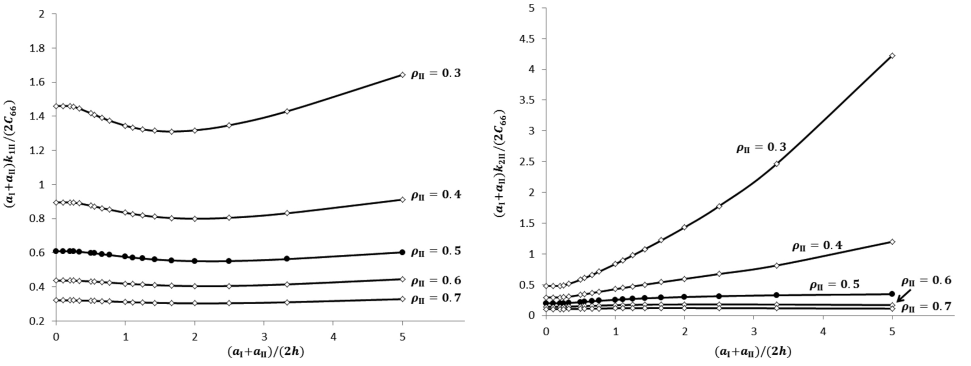

(a) (b)

Figure 6: Plots of $(a_I + a_{II})k_{1II}/(2C_{66}^{(2)})$ and $(a_I + a_{II})k_{2II}/(2C_{66}^{(2)})$ against $(a_I + a_{II})/(2h)$ for selected values of ρ_{II}

a/h increases, $ak_1/C_{66}^{(2)}$ increases if the half-spaces are occupied by martensite, but $ak_1/C_{66}^{(2)}$ becomes smaller if the half-spaces are occupied by e-glass-epoxy. In Fig. 7(b), the rate of increase in $ak_2/C_{66}^{(2)}$ with increasing a/h is the most drastic when the half-spaces are occupied by martensite. For a given a/h, Fig. 7 shows that the values of the effective coefficients for graphite-epoxy half-spaces are respectively smaller and larger than those for martensite and e-glass-epoxy half-spaces.

The observations above on the effective stiffness coefficients can be explained by noting the relative strength of the three materials selected for the analysis here. Martensite is the hardest of the three materials, whereas e-glass-epoxy is the soft-

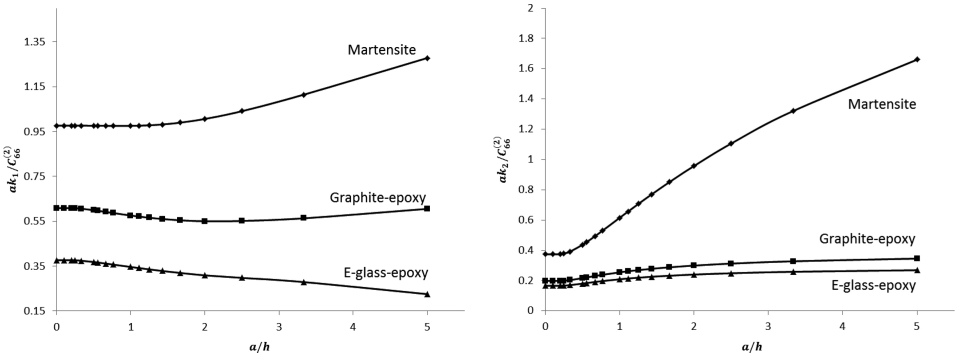

(a) (b)

Figure 7: Plots of $ak_1/C_{66}^{(2)}$ and $ak_2/C_{66}^{(2)}$ against a/h for the cases where martensite, graphite-epoxy and e-glass-epoxy are used as the material of the half-spaces

est. Thus, when the half-spaces are occupied by martensite, the trimaterial on the whole becomes stronger and the micro-cracks on the interfaces have relatively smaller displacement jumps over the micro-cracks, as a/h increases (that is, as the width of the layer decreases). At the same time, as a/h increases, the jump in the displacement u_2 over the micro-cracks also become smaller due to the shielding effect of parallel micro-cracks as explained in Case (b). All this combines to increase the effective stiffness coefficient k_2 of the interfaces drastically when the half-spaces are occupied by martensite. When the half-spaces are occupied by graphite-epoxy which is also the material in the layer, only the shielding effect of the parallel micro-cracks contributes to increasing the effective stiffness coefficient k_2 as a/h increases. For e-glass-epoxy half-spaces, increasing a/h has the effect of weakening the overall strength of the trimaterial, hence decreasing the effective stiffness coefficients. However, as shown in Fig. 7(b) for e-glass-epoxy, the effective stiffness k_2 may still increase with increasing a/h if the micro-crack shielding effect in increasing k_2 is more dominant than the opposing effect caused by the weakening of the trimaterial.

7 Summary

The present paper proposes a micromechanical model for estimating the effective stiffness coefficients of a pair of parallel weak interfaces in a trimaterial under inplane deformations. The trimaterial is made of an orthotropic thin layer sandwiched between two orthotropic half-spaces. The interfaces are microscopically damaged containing periodically distributed micro-cracks. The micromechanical model is formulated and numerically solved in terms of hypersingular boundary

integro-differential equations with the displacement jumps over the micro-cracks as unknown functions. Once the displacement jumps over the micro-cracks are obtained, the effective stiffness coefficients of the interfaces may be readily computed.

The case of a micro-cracked interface between an elastic half-space and a thin layer with one of its edges acted upon by prescribed tractions, as considered in Wang, Ang and Fan (2015), can be approximately recovered from the micromechanical model here by taking the upper interface of the trimaterial to be perfect and letting the upper half-space to be extremely soft. This provides a useful numerical check for the analysis here.

Some useful insights into the effects of the thin layer width, the elastic constants of the trimaterial and the interfacial micro-crack densities on the effective stiffness coefficients of the parallel interfaces are gained through specific case studies using particular orthotropic materials.

References

Ang, W. T. (2007): Elastodynamic antiplane deformation of a bimaterial with an imperfect viscoelastic interface: a dual reciprocity hypersingular boundary integral solution, *Applied Mathematical Modelling,* vol. 31, pp. 749-769.

Ang, W. T. (2013): *Hypersingular Integral Equations in Fracture Analysis*, Woodhead Publishing. Cambridge.

Abramowitz, M.; Stegun, I. (1970): *Handbook of Mathematical Functions*, Dover, New York.

Benveniste, Y.; Miloh, T. (2001): Imperfect soft and stiff interfaces in two-dimensional elasticity, *Mechanics of Materials*, vol. 33, pp. 309-323.

Berger, J. R.; Tewary, V. K. (2001): Green's functions for boundary element analysis of anisotropic bimaterials, *Engineering Analysis with Boundary Elements*, vol. 25, pp. 279-288.

Chen, E. L.; Ang, W. T. (2014): Green's functions and boundary element analysis for bimaterials with soft and stiff planar interfaces under plane elastostatic deformations, *Engineering Analysis with Boundary Elements*, vol. 40, pp. 50-61.

Clements, D. L. (1981): *Boundary Value Problems Governed by Second Order Elliptic Systems*, Pitman, London.

Fan, H.; Sze, K. Y. (2001): A micro-mechanics model for imperfect interface in dielectric materials, *Mechanics of Materials*, vol. 33, pp. 363-370.

Fan, H.; Wang, G. F. (2003): Interaction between a screw dislocation and viscoelastic interfaces, *International Journal of Solids and Structures*, vol. 40, pp. 763-776.

Gao, Z. W.; Lee, K. Y.; Zhou, Y. H. (2012): Crack tip shielding and anti-shielding effects of parallel cracks for a superconductor slab under an electromagnetic force, *Journal of Mechanical Science and Technology*, vol. 26, pp. 353-357.

Glodež, S.; Jezernik, N.; Kramberger, J.; Lassen,T. (2010): Numerical modelling of fatigue crack initiation of martensitic steel, *Advances in Engineering Software*, vol. 41, pp. 823-829.

Guechaichia, A.; Trendafilova, I. (2012): A simple frequency-based delamination detection and localization method without baseline model, *Journal of Physics: Conference Series*, vol. 382, pp. 012033.

Hashin, Z. (1991): The spherical inclusion with imperfect interface, *ASME Journal of Applied Mechanics*, vol. 58, pp. 444-449.

Jones, J. P.; Whittier, J. S. (1967): Waves at a flexibly bonded interface, *Journal of Applied Mechanics*, vol. 34, pp. 905-909.

Kaya, A. C.; Erdogan, F. (1987): On the solution of integral equations with strongly singular kernels, *Quarterly of Applied Mathematics,* vol. 45, pp. 105-122.

Knoll, W.; Advincula, R. C. (2011): *Functional Polymer Films*, Wiley-VCH, Weinheim.

Margetan, F. J.; Thompson, R. B.; Gray, T. A. (1988): Interfacial spring model for ultrasonic interactions with imperfect interfaces: Theory of oblique incidence and application to diffusion-bonded butt joints, *Journal of Nondestructive Evaluation*, vol. 7, pp. 131-152.

Muralt, P. (2000): Ferroelectric thin films for micro-sensors and actuators: a review, *Journal of Micromechanics and Microengineering*, vol. 10, pp. 136-146.

Purbolaksono, J.; Aliabadi, M. H. (2005): Dual boundary element method for instability analysis of cracked plates, *CMES: Computer Modeling in Engineering and Sciences*, vol. 8, pp. 73-90.

Rose, J. L. (1999): *Ultrasonic Waves in Solid Media*, Cambridge University Press, London.

Rubio-Gonzalez, C.; Mason, J. J. (2000): Dynamic stress intensity factors at the tip of a uniformly loaded semi-infinite crack in an orthotropic material, *Journal of the Mechanics and Physics of Solids*, vol. 48, pp. 899-925.

Sanz, J.; Solis, M.; Dominguez, J. (2007): Hypersingular BEM for piezoelectric solids: Formulation and applications for fracture mechanics, *CMES: Computer Modeling in Engineering and Sciences*, vol. 17, pp. 215-230.

Sudak, L. J.; Wang, X. (2006): Green's function in plane anisotropic bimaterials with imperfect interface, *IMA Journal of Applied Mathematics*, vol. 71, pp. 783-794.

Wang, X.; Ang, W. T.; Fan, H. (2015): Hypersingular integral and integro-differential micromechanical models for an imperfect interface between a thin orthotropic layer and an orthotropic half-space under inplane elastostatic deformations, *Engineering Analysis with Boundary Elements*, vol. 52, pp. 32-43.

Wang, X.; Ang, W. T.; Fan, H. (2012): Micro-mechanics models for an imperfect interface under anti-plane shear load: Hypersingular integral formulations, *Engineering Analysis with Boundary Elements*, vol. 36, pp. 1856-1864.

Wang, X.; Fan, H.; Ang, W. T. (2014): On micromechanical-statistical modeling of microscopically damaged interfaces under antiplane deformations, *International Journal of Solids and Structures*, vol. 51, pp. 2327-2335.